Journal of Nuclear Medicine, published on September 1, 2017 as doi:10.2967/jnumed.117.195073

# EVALUATION OF THE LYSOPHOSPHATIDIC ACID RECEPTOR TYPE 1 RADIOLIGAND $^{11}$C-BMT-136088 FOR LUNG IMAGING IN RHESUS MONKEYS

Authors: Jean-Dominique Gallezot[1], Nabeel B Nabulsi[1], Daniel Holden[1], Shu-Fei Lin[1], David Labaree[1], Jim Ropchan[1], Soheila Najafzadeh[1], David J Donnelly[2], Kai Cao[2], Samuel Bonacorsi[2], Jon Seiders[3], Jeffrey Roppe[3], Wendy Hayes[4], Yiyun Huang[1], Shuyan Du[4], Richard E Carson[1]

1 Radiology and Biomedical Imaging, Yale University, New Haven, CT, United States.
2 Discovery Chemistry Platforms, Bristol-Myers Squibb, Princeton, NJ, United States.
3 Amira Pharmaceuticals, San Diego, CA, United States.
4 Imaging, Bristol-Myers Squibb, Princeton, NJ, United States.

**Corresponding author**: Jean-Dominique Gallezot, Positron Emission Tomography (PET) Center, Yale University, 801 Howard Avenue, PO Box 208048, New Haven, CT 06520-8048. Phone: 1 203 737-9738. Fax: 1 203 785-3107. Email: jean-dominique.gallezot@yale.edu

Words: 4999

Running title: LPA1 radiotracer for lung imaging

**ABSTRACT**

The lysophosphatidic acid receptor type 1 (LPA1) is one of six known receptors of the extracellular signaling molecule LPA. It mediates effects such as cell proliferation, migration and differentiation. In the lung, LPA1 is involved in pathways leading, after lung tissue injury, to pulmonary fibrosis instead of normal healing, by mediating fibroblast recruitment and vascular leak. Thus, a LPA1 positron emission tomography (PET) radiotracer may be useful to study lung fibrosis, or to develop LPA1-targeting drugs. We developed and evaluated the novel radiotracer $^{11}$C-BMT-136088 (1-(4'-(3-methyl-4-(((1(*R*)-(3-$^{11}$C-methylphenyl)ethoxy)carbonyl)amino)isoxazol-5-yl)-[1,1'-biphenyl]-4-yl)cyclopropane-1-carboxylic acid) in rhesus monkeys, to image LPA1 in lung in vivo with PET. **Methods**: The study consists of three parts: test-retest scans; self-saturation to estimate the tracer's in vivo $K_D$, non-displaceable volume of distribution $V_{ND}$, and binding potential $BP_{ND}$; and dosimetry. In the first two parts, the radiotracer was administered using a bolus plus infusion protocol, the arterial input function was measured, and animals underwent two scans per day, separated by ~4 h. Lung regions of interest (ROIs) were segmented, and the tissue density estimated, from CT images. A fixed blood volume correction was applied. The tracer volume of distribution ($V_T$) was estimated using the multilinear analysis MA1 or equilibrium analysis (EA). **Results**: $^{11}$C-BMT-136088 baseline $V_T$ was 1.83±0.16 (MA1, $n$=5) or 2.1±0.55 (EA, $n$=7) mL plasma/g tissue in the bilateral lung ROI, with a test-retest variability of -6% (MA1, $n$=1) or -1±14% (EA, $n$=2). For the self-saturation study, $^{11}$C-BMT-136088 $V_{ND}$ and $BP_{ND}$ were estimated to be 0.9±0.08 mL plasma/g tissue and 1.1±0.14, respectively. The unlabeled drug dose (plasma concentration, respectively) leading to a 50% reduction of

$^{11}$C-BMT-136088 specific binding ($ID_{50}$) ($IC_{50}$, respectively) was 73±30 nmol/kg (28±12 nM, respectively). The average plasma free fraction was 0.2%, thus the tracer in vivo $K_D$ was estimated to be 55 pM. For the dosimetry study, the highest organ dose was observed in the liver (43.1±4.9 μSV/MBq and 68.9±9.4 μSv/MBq in reference human male and female phantoms, respectively), and the effective dose equivalent was 6.9±0.6 μSV/MBq in males and 8.7±0.6 μSv/MBq in females. **Conclusion**: Specific binding of $^{11}$C-BMT-136088 can be reliably measured to quantify LPA1 in the lungs of rhesus monkeys in vivo.

**Keywords**: Lysophosphatidic Acid Receptor Type 1, Lung, Positron Emission Tomography, Preclinical Imaging, Idiopathic Pulmonary Fibrosis.

## INTRODUCTION

Lysophosphatidic acid (LPA) is a glycerophospholipid serving as precursor for the formation of other phospholipids, and is an extracellular signaling molecule through a family of G-protein-coupled receptors (*1*). The lysophosphatidic acid receptor type 1 (LPA1) is a receptor encoded by one of the endothelial differentiation genes, EDG-2, which is widely expressed in the body, but with different levels of expression between organs, and between species (*2,3*). LPA signaling through LPA1 receptors has been linked to fibrosis in the lung (*4*), kidney (*5,6*) and liver (*7,8*), and LPA1 antagonists are currently under investigation as potential therapeutic drugs against fibrosis (*9*).

No radioligand was available to study LPA1 with positron emission tomography (PET). BMT-136088 is a high affinity and selective LPA1 antagonist (International patent applications PCT/US2012/032222 and PCT/US2014/063391). In this study, we report the first evaluation of $^{11}$C-BMT-136088 as a PET radioligand to quantify specific binding to LPA1 in lung. The body distribution and kinetics of $^{11}$C-BMT-136088 were evaluated, to estimate its radiation dosimetry.

## MATERIAL AND METHODS

### Study Plan and Population

This study consisted of three parts. The first part was a within-day test-retest study to evaluate the variability of $^{11}$C-BMT-136088 volume of distribution ($V_T$) (*10*) estimates, and verify that the duration of anesthesia does not induce a bias in $V_T$ estimates. The second part was a self-blocking study to quantify the fraction of specific binding of $^{11}$C-BMT-136088 and the tracer dose limit. The third part was a dosimetry study.

Two rhesus monkeys were included in the test-retest and self-blocking studies: one male, one female; age=4.8±0.8 y; weight=8.6±0.4 kg (all data are presented as mean±s.d., unless otherwise stated). Four animals were included in the dosimetry study (two males, two females; age=6.5±2.2 y; weight=7.6±10 kg). All experiments were conducted in accordance with the Yale University Institutional Animal Care and Use Committee guidelines.

### Radiochemistry

Figure 1 shows the radiolabeling of $^{11}$C-BMT-136088, prepared via Suzuki-Miyaura cross-coupling method by C–$^{11}$C-methylation of the aryl boronic ester precursor with $^{11}$C-methyl iodide, followed by hydrolysis of the carboxylate ester intermediate. The molar activity ($A_m$) at end of synthesis was 491±131 MBq/nmol (*n*=16; range: 81 – 634). The radiochemical purity was 99%±1% (*n*=16; range: 95% – 100%) and the chemical purity was 76%±20% (*n*=16; range: 27% – 96%). Details are described in the supplemental material.

**PET Data Acquisition**

PET scans were performed on a whole-body PET/CT scanner (Biograph mCT, Siemens Medical Systems, Erlangen, Germany).

For the test-retest and self-blocking studies, each monkey underwent two scans per day, with $^{11}$C-BMT-136088 injections 4.5±0.3 h apart. Following a low-dose CT scan for attenuation correction and delineation of the lung regions of interest (ROIs), $^{11}$C-BMT-136088 was injected with a bolus plus infusion protocol, with an initial 3-min bolus. The volume injected during the initial bolus represented 100 min ($K_{bol}$) worth of infusion in the test-retest study, and 300 min worth of infusion in the self-blocking study. The first test-retest study was performed using PE tubing to inject the radiotracer. After noticing that 29±2% of the activity was not injected but remained in the tubing, PTFE tubing was used to inject the tracer in all following studies. $K_{bol}$ was increased from 100 to 300 min in the self-blocking studies after analyzing the data from the second test-retest study (the first one with PTFE tubing) to re-optimize the bolus plus infusion protocol to achieve the flattest time-activity curves (*11*). With PTFE tubing, the activity lost in the injection line was negligible: 1±5%. $A_m$ at the time of injection (TOI) was 280±35 MBq/nmol ($n$=12). The injected dose was 126±45 MBq ($n$=12) and the injected mass was 40±19 ng/kg ($n$=7; for tracer dose studies only). For the self-blocking studies, lower $A_m$ was achieved by added unlabeled BMT-136088 to the injection syringe. The injected mass then ranged from 10 to 865 μg/kg for the non-tracer dose scans ($n$=5). Beginning at the start of each injection, a 120-minute time-of-flight list-mode acquisition was performed. Dynamic PET scan data were reconstructed with corrections for point-spread function, attenuation, normalization, scatter, randoms, and dead time using a 3D OP-

OSEM TOF algorithm. PET images were reconstructed into 33 frames (same timing as in (*12*)). Each frame contained 400×400×111 (x,y,z) voxels of size (2.04×2.04×2.0 $mm^3$).

For the dosimetry studies, following a low-dose CT scan used for attenuation correction, $^{11}$C-BMT-136088 was injected as a 1-min bolus. $A_m$ at TOI was 228±127 MBq, the injected activity was 135±30 MBq, and the injected mass was 84±89 ng/kg (*n*=4). Subjects were scanned for ~2 h in a sequence of 14 passes with 4 bed positions each, covering from the top of the head to mid-thigh.

**Arterial Blood Measurements**

Arterial blood samples were drawn from a catheter inserted in a limb artery to measure the whole blood and plasma radioactivity curves, the metabolite corrected plasma curve and the plasma free fraction ($f_P$) as previously described (*12,13*), with modifications for the high-performance liquid chromatography methods: see the supplemental material file for details. In one test-retest study, arterial blood sampling was not available and was replaced with venous blood sampling.

**ROI Delineation**

The lung ROIs were semi-automatically delineated using CT images collected before each PET scan: First, the lungs were segmented based on the Hounsfield scale (-1000<HU<-200), using a region growing algorithm and manually placed seeds; then the trachea was manually excluded, and slices that were ≤10 mm above the top of the liver dome were discarded; then the segmented lung ROIs were divided into right and left ROIs by manually selecting a sagittal plane.

Additional ROIs were drawn using CT images for the right atrium, and the right and left ventricles, the aorta, and the inferior (for leg vein injections) or superior (for arm vein injections) vena cava on early PET images (0-5 min post injection) to evaluate input functions for the lungs. An ROI was also drawn on the liver, the organ with the highest uptake.

**Density Correction for Lung ROIs**

It is critical to correct image data measured in the lung for the effect of tissue density, as shown in previous studies (*14*,*15*). Indeed, the time-activity curves (TACs) were originally computed for each ROI and expressed in kBq/cm$^3$. The lung ROI contains tissue, blood, and air, and net lung density can vary from scan to scan due to changes in animal positioning, e.g., due to changes in the left-right location of the heart, which can compress one side of the lungs and expand the other. Therefore, the density of lung ROIs was estimated to convert the lung TAC units from kBq/cm$^3$ to kBq/g, as follows. The CT images were converted from Hounsfield unit (*HU*) scale to linear attenuation values (in cm$^{-1}$) for 511 keV photons as described in (*16*). These attenuation values were assumed to be linearly proportional to mass for soft tissue and the heart density was assumed to be 1 g/cm$^3$. The size and the estimated density and mass of each lung ROI are listed in Supplemental Table 1.

**Quantification of Volumes of Distribution**

$V_T$ values were estimated using kinetic modeling and equilibrium analysis (EA). For kinetic modeling, three compartmental models and the multilinear analysis 1 (MA1) (*17*) were tested. The three compartmental models were the one- and two-tissue

compartment models (1TC and 2TC models), and a compartment model with one tissue compartment for $^{11}$C-BMT-136088 and one for all metabolites (1P1MC model). In that last model, all metabolites are assumed to enter and exit the tissue with the same rate constants. For the other models, it was assumed that no radioactive metabolites enter lung tissue. The MA1 method was modified to include a blood volume correction, using a fixed vascular fraction ($F_V$) of 0.5 based on the reported value of the extravascular lung mass to blood volume ratio of 0.92 in healthy humans (*18*). The operational equation for the modified MA1 method was:

$$C_{\mathrm{PET}}(t) = -\frac{V_{\mathrm{T}}}{b}\int_0^t C_{\mathrm{P}}(u)du + \frac{1}{b}\int_0^t C_{\mathrm{PET}}(u)du - \frac{F_{\mathrm{V}}}{b}\int_0^t C_{\mathrm{WB}}(u)du + F_{\mathrm{V}}C_{\mathrm{WB}}(t) \quad \text{Eq 1}$$

where $C_{\mathrm{PET}}$, $C_{\mathrm{P}}$ and $C_{\mathrm{WB}}$ denote the lung TAC (after density correction), the metabolite-corrected plasma TAC, and the whole-blood radioactivity TAC, respectively.

For EA, $V_{\mathrm{T}}$ was computed as follow:

$$V_{\mathrm{T}}^{\mathrm{EA}} = \frac{\int_{90}^{120}[C_{\mathrm{PET}}(t) - F_{\mathrm{V}} \times C_{\mathrm{WB}}(t)]dt}{\int_{90}^{120} C_{\mathrm{P}}(t)dt} \quad \text{Eq 2}$$

In all analyses, the arterial whole blood and metabolite-corrected plasma curves were corrected for the delay ($\delta$) between the right ventricle and the arterial sampling point. $\delta$ was estimated by fitting the right ventricle curve with a shifted and scaled arterial blood curve:

$$C_{RV}(i) = A\int_{t_i}^{t_i+\Delta t_i} C_{WB}(t+\delta) \quad \text{Eq 3}$$

where $i$, $C_{RV}$, $A$, $t_i$, $\Delta t_i$ represent the frame index, the right ventricle TAC, scale factor, frame start time, and frame duration, respectively. $\delta$ and $A$ were estimated to be 6.1±3.6 seconds and 1.11±0.07, respectively.

**Test-Retest Variability of $^{11}$C-BMT-136088 $V_T$ Estimates**

The within-day variability of $^{11}$C-BMT-136088 $V_T$ estimates, was estimated by computing the test-retest variability TRV as:

$$TRV = 2 \times \frac{V_T^{Retest} - V_T^{Test}}{V_T^{Retest} + V_T^{Test}} \quad \text{Eq 4}$$

The between-day variability of $^{11}$C-BMT-136088 $V_T$ estimates was estimated by computing the average within-subject and within-ROI coefficient of variation (COV) across tracer dose (non-blocking) studies on different days.

**Analysis of $^{11}$C-BMT-136088 Self-Blocking Study**

The $ID_{50}$ ($IC_{50}$, respectively) of $^{11}$C-BMT-136088 was estimated by plotting the estimated $V_T$ values versus the injected masses (BMT-136088 plasma concentrations, respectively) of BMT-136088 and fitting the resulting curves with the following models:

$$V_T = V_{ND} + V_S \times \frac{ED_{50}}{ED_{50} + dose_{drug}} \quad \text{Eq 5}$$

$$V_T = V_{ND} + V_S \times \frac{IC_{50}}{IC_{50} + [drug]_{plasma}} \quad \text{Eq 6}$$

where $V_{ND}$ is the non-displaceable volume of distribution, and $V_S$ is the specific volume of distribution (*10*). The binding potential $BP_{ND}$ (*10*) was computed from these two parameters as $V_S$ / $V_{ND}$. Data for each monkey and each lung (right or left) were analyzed separately or together to determine if they were compatible with a single model (using the *F*-test for statistical analysis).

## RESULTS

### Blood Compartment

The distribution of radioactivity in the body after a baseline injection of $^{11}$C-BMT-136088 is shown in Figure 2. The radioactivity curves in arterial whole blood and plasma are shown in Figure 3, as well as the fraction of unchanged $^{11}$C-BMT-136088 in arterial plasma and the metabolite-corrected arterial plasma concentration. The whole blood to plasma radioactivity ratio was 1.18±0.27 at the beginning of the scans (0-3 min post injection, $n$=10) and 1.05±0.15 at the end of the scans (90-120 min post injection, $n$=10). The unchanged fraction was 91%±3% ($n$=10) at 3 min post injection, 75%±3% ($n$=10) at 30 min post injection and 59%±6% ($n$=10) at 90 min post injection. The plasma free fraction $f_P$ was very low, at 0.19%±0.06% ($n$=10).

### Tissue Compartments

The density, estimated using the CT images, of the right and left lung ROIs was 0.33±0.02 g/cm$^3$ and 0.32±0.01 g/cm$^3$, respectively, in one monkey ($n$=6), and 0.46±0.04 g/cm$^3$ and 0.42±0.03 g/cm$^3$, respectively, in the second monkey ($n$=6).

Time activity curves for the lung, liver and heart from tracer doses studies are shown in Figure 4. The highest uptake was seen in the liver: SUV was 18±4.7 during the 30 – 120 min post injection interval ($n$=7). During the same interval, the SUV in lung was 1.2±0.15 on both sides (density corrected values). The percentage change per hour (computed over the 30 – 120 min pi interval) was -5±17, -3±17, -11±18 and -11±16 %/hr in the right and left lungs, liver and heart, respectively ($n$=12). It was -23±19 %/hr ($n$=10)

for the metabolite-corrected arterial plasma concentration. Thus, equilibrium was apparently reached in the lung in average, but not in the arterial plasma.

**Kinetic Modeling**

Representative fits obtained with the 1TC and 2TC models (which assume only parent tracer enters the lungs) and the 1P1MC model (with one metabolite compartment) are shown in Figure 5.

Better fits were obtained with the 2TC model than with the 1TC and 1P1MC models: the reduced residual sum of squares and the Akaike information criterion were always lower for the 2TC model than for the 1TC model ($p<0.0001$, Wilcoxon matched-pairs signed rank test, $n=20$, for both metrics); the same metrics were lower for the 2TC model than for the 1P1MC model 16 times out of 20 lung TAC fits ($p<0.005$, Wilcoxon matched-pairs signed rank test, $n=20$). However, due to the complexity of the 2TC model (4 estimated parameters), the $V_T$ estimates were not precise (%SE were 5%-60%, with a median value of 7%). Thus, we tested the multilinear analysis MA1, which provides a compromise between the accuracy of fits and stability of parameter estimates ($V_T$ %SE were 1%-7%, with a median value of 2%). Due to the high fraction of blood in the lungs, a modified version of MA1 was used, incorporating a fixed (50% by mass) correction for blood radioactivity. The average $V_T$ estimates in right and left lungs were 1.8±0.19 and 1.9±0.13 mL/g, respectively, for tracer doses studies ($n=5$). The average 2TC $K_1$ estimates at baseline in right and left lungs were 0.33±0.26 and 0.35±0.32 mL/min/g, respectively.

EA was also tested to quantify $V_T$. EA tended to overestimate $V_T$ compared to MA1. The mean EA $V_T$ in right and left lungs were 2.1±0.55 and 2.1±0.56 mL/g, respectively, for tracer doses studies ($n$=7). The slope of the regression line between EA $V_T$ values and MA1 $V_T$ values is 1.21±0.23 (intercept=-0.04±0.35, $r^2$=0.611, $n$=20).

**Test-Retest Study**

The within-day test-retest variability of $V_T$ with MA1 could only be estimated in one monkey, due to missing arterial data in the other animal. In this animal, the TRV was -8% and -5% in the right and left lung ROIs, respectively. With EA, TRV was computed in both animals, using venous data for the animal missing arterial data. TRV was -1%±11% and -2%±10% in the right and left lung, respectively. The between-day COV of $^{11}$C-BMT-136088 $V_T$ estimates was 10% with MA1 and 17% with EA. Due to this lower COV, MA1 was the method selected for the analysis of $^{11}$C-BMT-136088 (self-) saturation study. The excess variability of EA $V_T$ values, and the fact that EA $V_T$ values were higher that MA1 $V_T$ values, is likely due to fact that the tracer concentration could not be made constant in the plasma and the lung at the same time, violating EA hypotheses.

**Saturation Study**

The relationship between the mass of $^{11}$C-BMT-136088 administered during the saturation study and the plasma levels of $^{11}$C-BMT-136088 was linear, with a slope of 0.92 nM / (μg/kg) ($r^2$=0.999, $n$=5) (Supplemental Fig. 1A) and thus, the relationship between $^{11}$C-BMT-136088 $V_T$ and $^{11}$C-BMT-136088 injected mass (Supplemental Fig. 1B) is visually very similar to the relationship between $^{11}$C-BMT-136088 $V_T$ and

$^{11}$C-BMT-136088 plasma levels (Fig. 6). Both relationships could be fitted with a one-saturable-site model, with identical parameters for both animals and both lung ROI (right and left) (*F*-test statistics were $F_{9,4}$=0.24, $p$=0.96 for $V_T$ versus mass, and $F_{9,4}$=0.26, $p$=0.93 for $V_T$ versus plasma concentration). The $IC_{50}$ and $ID_{50}$ of $^{11}$C-BMT-136088 were estimated to be 28±12 nM and 36±15 µg/kg, respectively. Using the average $f_P$ value of 0.19%, the in vivo $K_D$ of $^{11}$C-BMT-136088 was computed as 55 pM. $V_{ND}$ was estimated to 0.9±0.93 mL/g and $BP_{ND}$ was estimated to 1.1±0.14, meaning that specific binding of $^{11}$C-BMT-136088 in the lung represents 52% of the (blood contribution corrected) radioactivity concentration in the lung at equilibrium.

**Dosimetry**

Dosimetry studies were analyzed as previously described (*19*). Supplemental Table 2 shows the mean absorbed doses. Under CFR 361.1.1 the liver is the dose limiting organ with single study dose limit of 1160 MBq for a male and 726 MBq for a female. Thus, multiple injections can be performed in healthy subjects per year.

## DISCUSSION

In this study, we evaluated the properties of the novel radiotracer $^{11}$C-BMT-136088 to image LPA1 receptors in lung. We used quantitative modeling techniques, accounting for lung blood volume and found that the tracer binds to LPA1 and that we could determine the in vivo $K_d$ and the tracer's $BP_{ND}$.

Arterial data, sampled from a limb artery, was used as the input function for modeling. This is not the actual input function for the lung, which should ideally be measured from the pulmonary artery or the right ventricle. However, due to this tracer properties, arterial data is a reasonable alternative lung input function. First, the image-derived whole blood TACs from right and left ventricle were very similar (Supplemental Fig. 2), due to the low uptake for this tracer in the lung: $K_1$ was ~0.3 mL/min/g; For comparison, in un-anesthetized human subjects at rest, pulmonary perfusion measured with $^{15}$O-water is ≥1.2 mL/min/mL (*20*,*21*) which would be ≥ 3.0 mL/min/g assuming a lung density of 0.40 g/mL. In anesthetized pigs, pulmonary blood flow was estimated to be 0.59 mL/min/mL (or 1.5 mL/min/g assuming lung density of 0.40 g/mL) (*22*). Thus, the exit curve (i.e., the left ventricle TAC, and subsequently limb arterial data) is similar to the input curve (i.e., the right ventricle). The inferior vena cava is another promising ROI to measure the lung input function if the radiotracer is injected in a leg vein (Supplemental Fig. 2).

For imaging studies outside of the brain, the possibility of metabolites entering the tissue should be considered. In this study, we tested a simple model with 1 tissue-compartment for the parent tracer and 1 tissue-compartment for metabolites. This model did not provide good fits, implying than more compartments are needed for parent and/or

metabolites. However, such models would be too complex to obtain stable $V_T$ estimates. Moreover, it is unlikely that these models could be used without *a priori* data about the parent fraction in tissue, which can only be obtained with ex-vivo measurements.

For studies in lung, density correction is critical to obtain reproducible and reliable data. Density correction was especially important due to the effects of animal positioning on the position of the heart in rhesus monkeys; this led to different compression/expansion of the right and left lungs from scan to scan. In future studies involving idiopathic pulmonary fibrosis (IPF) patients, or animal models, density correction would also be needed to take into account the increased density in the diseased state (*14,15*). In this study, density correction was based on CT data, which was acquired over the duration of 1-2 breathing cycles, and applied on a whole-ROI basis. For studies in humans, care should be taken to obtain CT data representative of an average, whole cycle, to match the PET data, or from a fixed and reproducible part of the cycle in order to minimize breathing-based variability in the density correction. Methods have been proposed to co-register two CT images taken at different parts of the breathing cycle, and preserve the lung tissue mass during that registration (*23*), however it is simplest if such mismatch is avoided whenever possible. For parametric imaging of the lung, it is likely than even more care would be needed to obtain reliable per voxel density estimates (*15*).

A final correction that is needed in lung studies is to account for blood radioactivity. Indeed, blood volume in lung is high, with about 50% of the total mass of lungs attributed to blood: using $^{11}$C-CO, Rhodes et al. measured an extravascular lung to blood volume ratio of 0.92 in healthy humans (*18*), which translates to a fractional mass of blood of 52%. Thus, blood volume correction is potentially needed for all tracers in

lung. Here, the radioactivity concentration of $^{11}$C-BMT-136088 in whole blood was of the same order of magnitude as that of $^{11}$C-BMT-136088 in lung (SUV were 0.74±0.13 in blood versus 1.2±0.15 in lung for tracer doses studies), thus blood volume correction has a large effect on the data. In addition, in the blockade studies, drug administration tended to increase radioactivity in whole blood, which would have reduced the apparent reduction of $^{11}$C-BMT-136088 $V_T$ values if blood volume correction was not applied. These last two properties of $^{11}$C-BMT-136088 make blood volume correction especially important for this tracer. In this study, we used a fixed $F_V$ value of 0.5 mL/g, as it is the typical fraction of blood in lung by mass previously estimated in healthy humans. This value was also close to the average fitted value (0.52 ± 0.22 mL/g) obtained when $F_V$ was estimated in 1TC fits of the first 11 minutes of lung TACs.

The presence of saturable (displaceable) signal could be verified with the self-blocking study, and $^{11}$C-BMT-136088 is a high affinity LPA1 antagonist in vitro. However, future work is still needed to verify its selectivity in vivo, using well-characterized, subtype selective, antagonists for various LPA receptors to block $^{11}$C-BMT-136088 binding.

This study shows that $^{11}$C-BMT-136088 is a potentially useful radioligand to image LPA1 receptors in the lung. However, human studies will be needed to confirm its suitability. Density of LPA1 in healthy humans is unknown, but EDG-2 expression is detectable in healthy humans (*2*), though relatively low compared to other organs. In IPF, the concentration of LPA is increased in the bronchoalveolar lavage fluid, and LPA1-expressing fibroblasts are present, while they are absent in healthy controls (*4*). Thus, $^{11}$C-BMT-136088 may be a useful tracer to detect potential upregulation of LPA1

receptors in the lungs of IPF patients. One caveat is that IPF is most prevalent in lower lung at the beginning of the disease (*24*,*25*), so correction of respiratory motion will be needed, and spill-in from liver could affect quantification.

Future studies in rodents are also needed to evaluate the usefulness of $^{11}$C-BMT-136088 in animal models of IPF (*26*). One drawback of $^{11}$C-BMT-136088 is its high uptake in the liver, which makes PET quantification difficult in the lower parts of the monkey lung, and which will be worse in smaller animals if high liver uptake is also seen in these species. $^{11}$C-BMT-136088 may also be useful to study the involvement of LPA1 receptors in fibrosis in other organs than the lung, such as the kidney where LPA1 activation has been shown to promote interstitial fibrosis (*6*).

Finally, since $^{11}$C-BMT-136088 specific binding is clearly saturable with a $BP_{ND}$ of ~1.1, this study showed that $^{11}$C-BMT-136088 is a suitable radioligand to verify target engagement and quantify the $IC_{50}$ or $ID_{50}$ of drugs targeting LPA1 in preclinical studies in rhesus monkeys.

## CONCLUSION

$^{11}$C-BMT-136088 is the first available radioligand for quantifying the density of LPA1 receptors in lung with PET. It is also suitable to conduct preclinical drug occupancy studies in rhesus monkeys. These findings warrant further evaluation of this radioligand in animal models of fibrosis and in patients.

**REFERENCES**


**1.** Kihara Y, Maceyka M, Spiegel S, Chun J. Lysophospholipid receptor nomenclature review: IUPHAR Review 8. *Br J Pharmacol.* 2014;171:3575-3594.

**2.** An S, Bleu T, Hallmark OG, Goetzl EJ. Characterization of a novel subtype of human G protein-coupled receptor for lysophosphatidic acid. *J Biol Chem.* 1998;273:7906-7910.

**3.** Contos JJ, Ishii I, Chun J. Lysophosphatidic acid receptors. *Mol Pharmacol.* 2000;58:1188-1196.

**4.** Tager AM, LaCamera P, Shea BS, et al. The lysophosphatidic acid receptor LPA1 links pulmonary fibrosis to lung injury by mediating fibroblast recruitment and vascular leak. *Nat Med.* 2008;14:45-54.

**5.** Pradère J-P, Gonzalez J, Klein J, et al. Lysophosphatidic acid and renal fibrosis. *Biochim Biophys Acta.* 2008;1781:582-587.

**6.** Pradère J-P, Klein J, Grès S, et al. LPA1 receptor activation promotes renal interstitial fibrosis. *J Am Soc Nephrol.* 2007;18:3110-3118.

**7.** Ikeda H, Yatomi Y, Yanase M, et al. Effects of lysophosphatidic acid on proliferation of stellate cells and hepatocytes in culture. *Biochem Biophys Res Commun.* 1998;248:436-440.

**8.** Watanabe N, Ikeda H, Nakamura K, et al. Both plasma lysophosphatidic acid and serum autotaxin levels are increased in chronic hepatitis C. *J Clin Gastroenterol.* 2007;41:616-623.

**9.** Rancoule C, Pradère J-P, Gonzalez J, et al. Lysophosphatidic acid-1-receptor targeting agents for fibrosis. *Expert Opin Investig Drugs.* 2011;20:657-667.

**10.** Innis RB, Cunningham VJ, Delforge J, et al. Consensus nomenclature for in vivo imaging of reversibly binding radioligands. *J Cereb Blood Flow Metab.* 2007;27:1533-1539.

**11.** Carson RE, Channing M, Blasberg R, et al. Comparison of bolus and infusion methods for receptor quantitation: application to [18F]cyclofoxy and positron emission tomography. *J Cereb Blood Flow Metab.* 1993;13:24-42.

**12.** Lin S-F, Labaree D, Chen M-K, et al. Further evaluation of [11C]MP-10 as a radiotracer for phosphodiesterase 10A: PET imaging study in rhesus monkeys and brain tissue metabolite analysis. *Synapse.* 2015;69:86-95.

**13.** Hannestad J, Dellagioia N, Gallezot J-D, et al. The neuroinflammation marker translocator protein is not elevated in individuals with mild-to-moderate depression: a [$^{11}$C]PBR28 PET study. *Brain Behav Immun.* 2013;33:131-138.

**14.** Holman BF, Cuplov V, Millner L, et al. Improved correction for the tissue fraction effect in lung PET/CT imaging. *Phys Med Biol.* 2015;60:7387-7402.

**15.** Lambrou T, Groves AM, Erlandsson K, et al. The importance of correction for tissue fraction effects in lung PET: preliminary findings. *Eur J Nucl Med.* 2011;38:2238-2246.

**16.** Carney JPJ, Townsend DW, Rappoport V, Bendriem B. Method for transforming CT images for attenuation correction in PET/CT imaging. *Medical physics.* 2006;33:976-983.

**17.** Ichise M, Toyama H, Innis RB, Carson RE. Strategies to improve neuroreceptor parameter estimation by linear regression analysis. *J Cereb Blood Flow Metab.* 2002;22:1271-1281.

**18.** Rhodes CG, Wollmer P, Fazio F, Jones T. Quantitative measurement of regional extravascular lung density using positron emission and transmission tomography. *J Comput Assist Tomo.* 1981;5:783-791.

**19.** Naganawa M, Waterhouse RN, Nabulsi NB, et al. First in human assessment of the novel PDE2A PET radiotracer 18F-PF-05270430. *J Nucl Med.* 2016.

**20.** Heinonen I, Savolainen AM, Han C, et al. Pulmonary blood flow and its distribution in highly trained endurance athletes and healthy control subjects. *J Appl Physiol.* 2013;114:329-334.

**21.** Schuster DP, Kaplan JD, Gauvain K, Welch MJ, Markham J. Measurement of regional pulmonary blood flow with PET. *J Nucl Med.* 1995;36:371-377.

**22.** Neeb D, Kunz RP, Ley S, et al. Quantification of pulmonary blood flow (PBF): validation of perfusion MRI and nonlinear contrast agent (CA) dose correction with H(2)15O positron emission tomography (PET). *Magn Reson Med.* 2009;62:476-487.

**23.** Yin Y, Hoffman EA, Lin C-L. Mass preserving nonrigid registration of CT lung images using cubic B-spline. *Medical physics.* 2009;36:4213-4222.

**24.** American Thoracic Society/European Respiratory Society International Multidisciplinary Consensus Classification of the Idiopathic Interstitial Pneumonias. *Am. J. Respir. Crit. Care Med.* Vol 165; 2002:277-304.

**25.** Idiopathic pulmonary fibrosis: diagnosis and treatment. International consensus statement. *Am. J. Respir. Crit. Care Med.* Vol 161; 2000:646-664.

**26.** Della Latta V, Cecchettini A, Del Ry S, Morales MA. Bleomycin in the setting of lung fibrosis induction: from biological mechanisms to counteractions. *Pharmacol Res.* 2015;97:122-130.

**FIGURES**

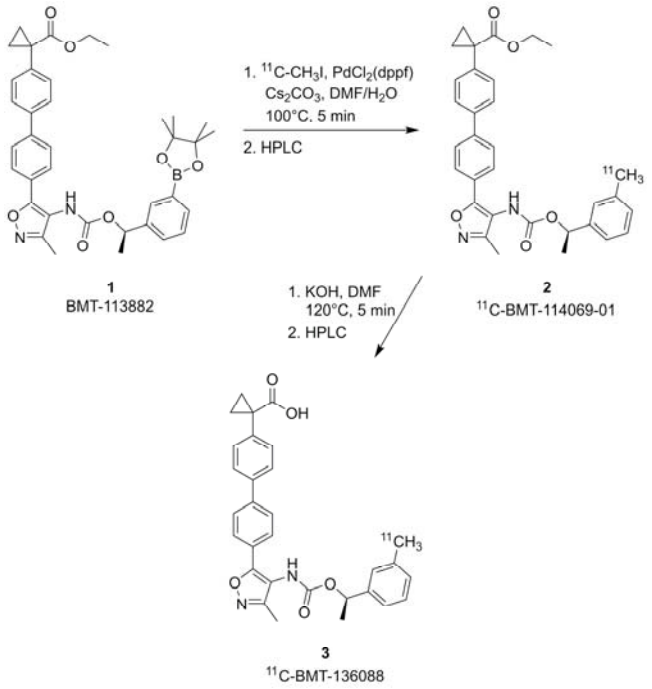


**Figure 1**: Radiosynthesis of $^{11}C$-BMT-136088

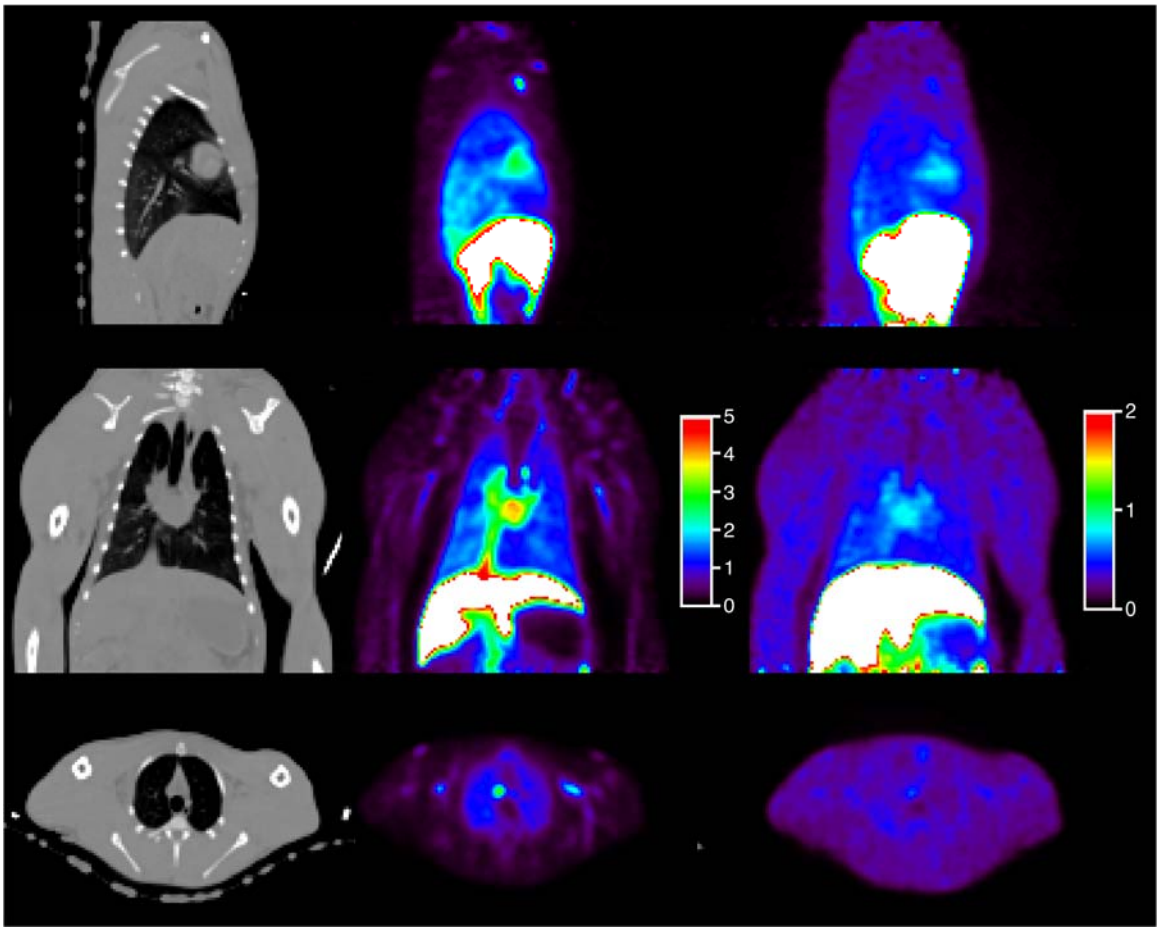


**Figure 2:** Images of $^{11}$C-BMT-136088 distribution: CT images (left), early (0-5 min post injection, center) and late (40-60 min post injection, right) distribution, expressed in SUV, in sagittal, coronal and transverse views (from top to bottom).

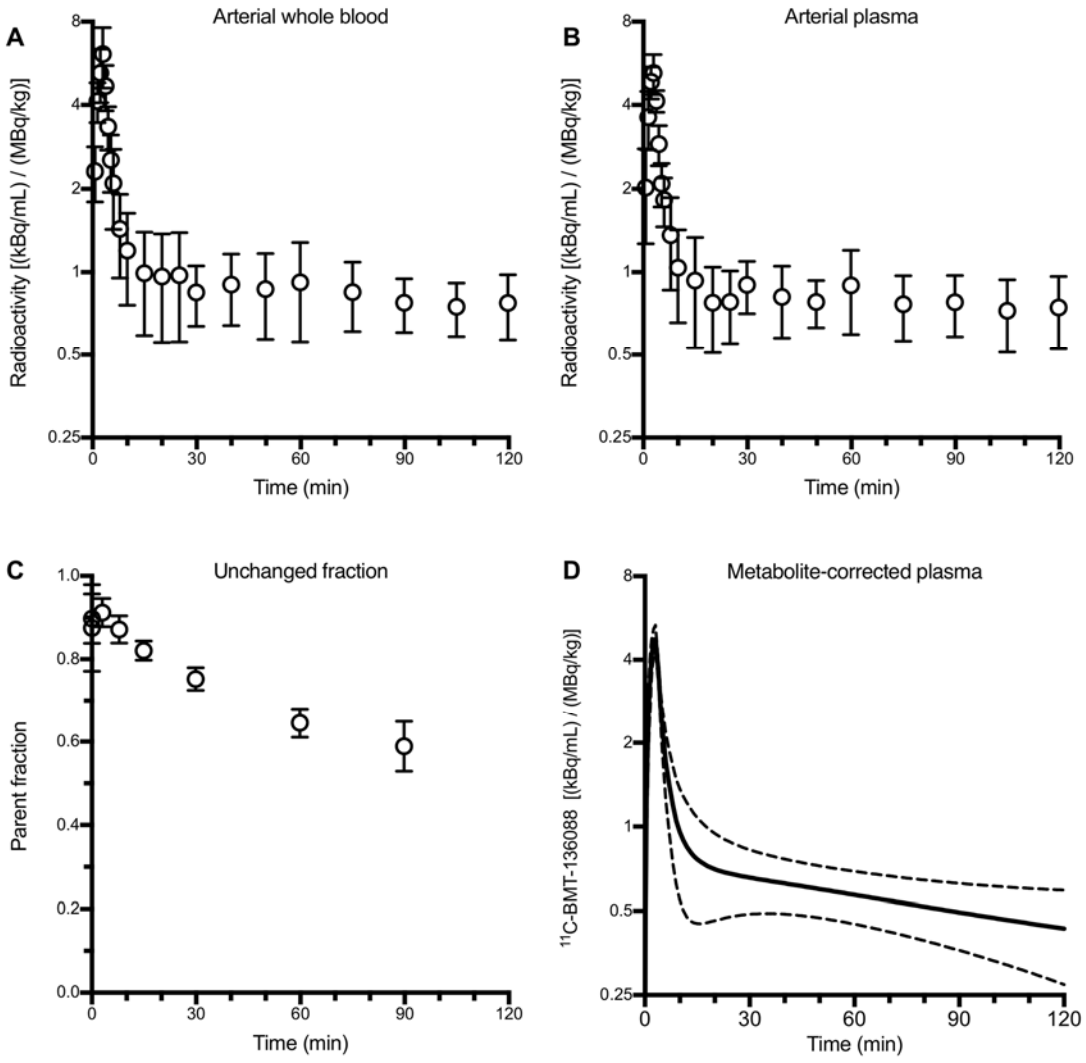


**Figure 3**: Average whole blood (**A**), plasma (**B**), unchanged fraction (**C**) and metabolite corrected plasma (**D**) curves (*n*=10 scans with arterial blood sampling). Error bars (**A** to **C**) or dashed lines (**D**) represent standard deviation across studies.

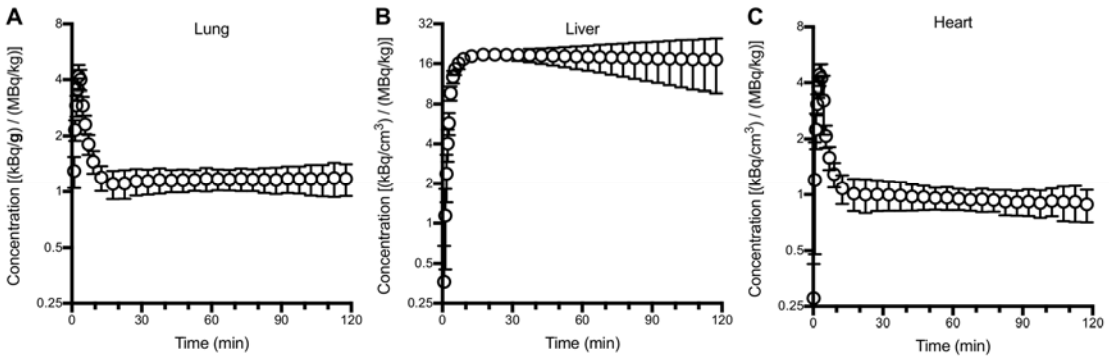


**Figure 4**: (**A**) Lung, (**B**) liver and (**C**) heart TACs from tracer doses studies (*n*=7). Error bars represent standard deviation across studies.

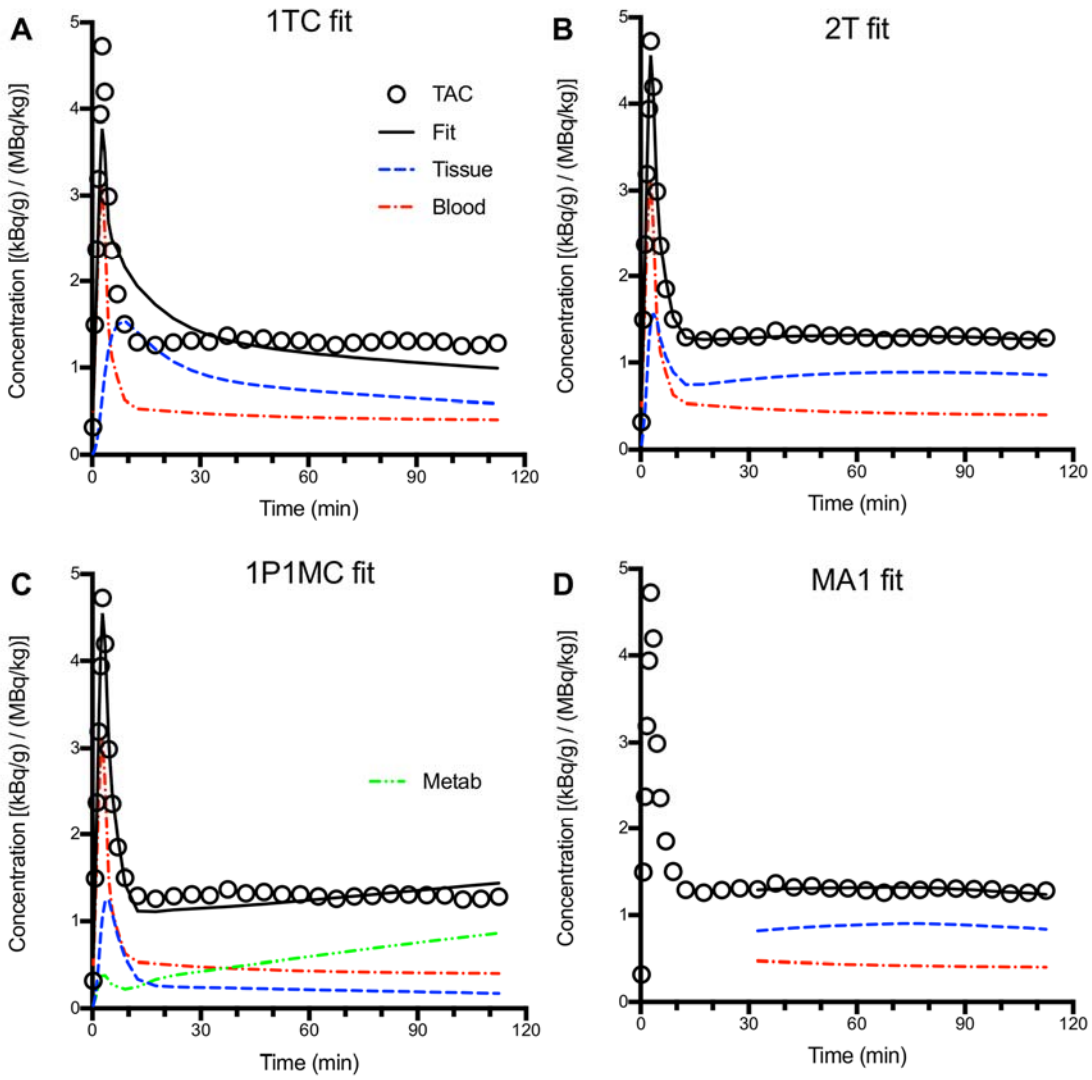


**Figure 5**: Model fits of lung TACs: 1TC (**A**), 2TC (**B**), 1P1MC (**C**) and MA1 with blood volume correction (**D**) fits. Open circles represent measured PET data, solid black lines represent the best fit, dashed red lines represent the blood contribution, and blue dashed lines represent the modeled (parent) activity in the lung tissue. In (**C**), the green dashed line represents the modeled activity in the lung due to metabolites.

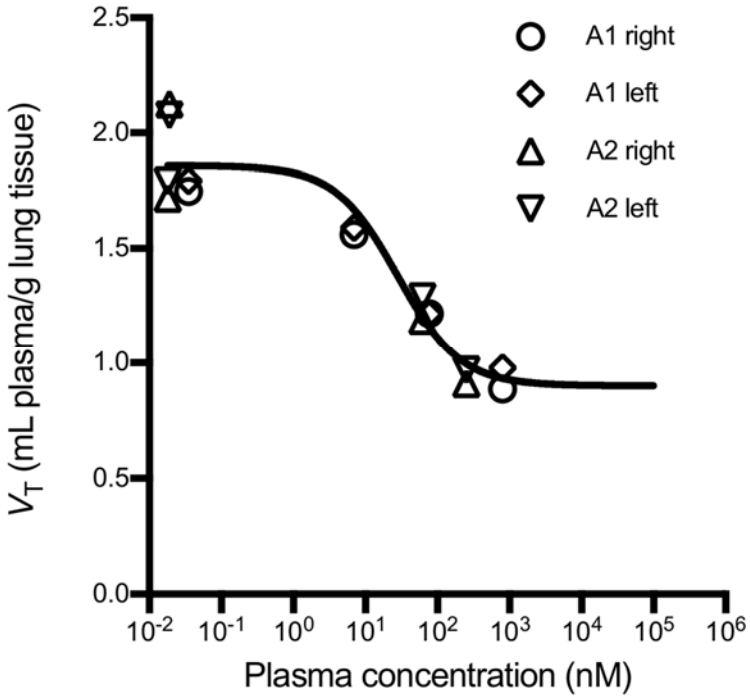


**Figure 6**: Relationship between $^{11}$C-BMT-136088 $V_T$ values and the plasma levels of BMT-136088. The data from both animals (A1 and A2) and from both sides (right and left) of the chest could be fitted by the same curve. The solid line represents the fit to Eq. 6.

**Radiochemistry**

**$^{11}$C-BMT-136088 [1-(4'-(3-methyl-4-((((*R*)-1-(3-$^{11}$C-methylphenyl)ethoxy)-carbonyl)amino)isoxazol-5-yl)-[1,1'-biphenyl]-4-yl)cyclopropane-1-carboxylic acid] (3)**

The following radio-HPLC systems were used: a preparative HPLC system including a Shimadzu LC-20A pump, a Rheodyne 7133i injector with a 2-mL loop, a Knauer K200 ultraviolet detector, a Bioscan $\gamma$ -flow detector, and a laptop computer running the EZStart data acquisition software; an analytic HPLC system consisting of a Shimadzu LC-20A quaternary pump, a Rheodyne 7133i injector, a Shimadzu SPD-M20A PDA or SPD-20A ultraviolet detector, a flow cell $\gamma$ detector (Bioscan), and a PC with Shimadzu Class VP 7.2 software used for system control.

$^{11}CO_2$ was produced through the $^{14}N(p, \alpha)^{11}C$ nuclear reaction by bombardment of a high-pressure target containing a mixture of nitrogen and oxygen (0.5%–1%) with a 16.8-MeV proton beam that was produced by the PETTrace cyclotron (GE Healthcare) cyclotron. $^{11}$C-Methyl iodide was synthesized by the gas-phase method from $^{11}CO_2$ using the FXMeI or the FXC module (GE Healthcare), by reduction of $^{11}CO_2$ with hydrogen on SHIMSHIMALITE nickel to $^{11}$C-methane, followed by iodination at 720 °C (*1*). Then $^{11}$C-methyl iodide was swept with helium at 20 mL/min into an acetone/ice bath-cooled reaction vial containing a solution of the boronic ester precursor **1** (2.5-3 mg) along with a catalytic amount of the palladium catalyst, [1,1'-bis(diphenylphosphino)ferrocene]-dichloropalladium(II), $Pd(dppf)Cl_2$, (0.8-1.2 mg), and cesium carbonate (3-4 mg) in 4:1 *N,N*-dimethylformamide (DMF):water. The reaction vial was then heated while stirring at

100 ºC for 5 min. The resulting solution was cooled, diluted with ~1.7 mL of the semipreparative HPLC buffer solution of the intermediate **2**, and then purified by semipreparative HPLC (Gemini C18, 5μ, 75:25 acetonitrile:0.1 M ammonium formate containing 0.5% acetic acid of pH 4.2-4.3, and flow rate of 2 mL/min for 3 min, followed by 5 mL/min). The radioactive intermediate **2** fraction ($t_R$13-14 min) was collected in a plastic syringe containing 10 mL of dionized (DI) water, and then was loaded onto a Waters C18 SepPak. After drying the SepPak with argon gas, the trapped radioactive intermediate **2** was eluted of the SepPak with 1-1.2 mL DMF into a reaction vial containing 400 μL of 12 N KOH, and the mixture was heated at 100° C for 5 min. The resulting solution was cooled, then diluted with a mixture of 250 μL of acetic acid and 500 μL of the semipreparative HPLC buffer solution of **3** (*vide infra*), and then purified by semipreparative HPLC (Luna C18, 5μ, 70:30 ethanol (190 proof, USP grade):saline (USP grade) containing 0.5% acetic acid of pH 3.2, and flow rate of 5 mL/min). The desired radioactive product **3** fraction was collected ($t_R$ 5-6 min) into a sterile syringe barrel containing 2 mL USP saline, and the resulting mixture was then passed through a sterile membrane filter (0.22 μm) for terminal sterilization, and collected in a sterile vial containing 18 mL of sterile USP saline and 100 μL of sterile USP sodium bicarbonate (4.2%) to afford a formulated IV solution of $^{11}$C-BMT-136088 **3** ready for dispensing and administration. Chemical purity, radiochemical purity, and molar activity of **3** were determined by HPLC analysis of the product solution (column: Phenomenex Prodigy C18, 5 μm, 100Å, 4.6 × 250 mm; mobile phase: 60% acetonitrile and 40% 0.1 M aqueous ammonium formate solution containing 0.5% acetic acid, pH 4.2; flow rate: 2 mL/min;

UV detector wavelength: 300 nm). The identity of $^{11}$C-BMT-136088 was confirmed by coinjection of the radiolabeled product with unlabeled BMT-136088.

**HPLC methods for metabolite correction**

Aliquots of plasma drawn at 3, 8, 15, 30, 60 and 90 min post-injection were further processed by HPLC to quantify $^{11}$C-BMT-136088 parent fraction, using the column-switching method (*2*). Briefly, aliquots were treated with urea (8 M) and then filtered through 1.0 μm Whatman 13 mm GD/X syringe filters (GE, Florham Park, NJ, USA) for metabolite analysis. Up to 6 mL of plasma filtrate was injected onto the automatic column-switching HPLC system equipped with a capture column (19 x 4.6 mm) packed with Phenomenex SPE C18 Strata-X sorbent (Torrance, CA, USA) and eluting with 1% acetonitrile in water at a flow rate of 2 mL/min. After 4 min, activity trapped on the capture column was back-eluted onto a Phenomenex Luna C18 (2) analytical column (5 μm, 4.6 x 250 mm) eluting with a mobile phase of 52.5% acetonitrile and 47.5% 0.1 M ammonium formate (v/v) at a flow rate of 1.75 mL/min. HPLC eluate was fraction-collected and the fractions were measured with gamma well counters.

**References**

**1.** Larsen P, Ulin J, Dahlstrøm K, Jensen M. Synthesis of [11C]iodomethane by iodination of [11C]methane. *Appl Radiat Isot.* 1997;48:153-157.

**2.** Hilton J, Yokoi F, Dannals RF, Ravert HT, Szabo Z, Wong DF. Column-switching HPLC for the analysis of plasma in PET imaging studies. *Nucl Med Biol.* 2000;27:627-630.

## Lung ROI volumes and densities

**Supplemental Table 1:** volumes, densities and masses of lung ROIs for each scan

| | | | Lung ROI volume (mL) | | | Lung ROI density (g/mL) | | | Lung ROI mass (g) | | |
|---|---|---|---|---|---|---|---|---|---|---|---|
| Scan number | Study | Animal | left | Right | Bilateral | left | Right | Bilateral | left | Right | Bilateral |
| 1 | Test-Retest | 1 | 96 | 122 | 218 | 0.328 | 0.302 | 0.313 | 31.5 | 36.9 | 68.4 |
| 2 | | 1 | 91 | 126 | 217 | 0.339 | 0.311 | 0.323 | 30.9 | 39.3 | 70.2 |
| 3 | | 2 | 97 | 74 | 171 | 0.420 | 0.515 | 0.461 | 40.8 | 37.9 | 78.7 |
| 4 | | 2 | 89 | 102 | 191 | 0.425 | 0.436 | 0.431 | 37.9 | 44.5 | 82.4 |
| 5 | Saturation | 1 | 118 | 125 | 242 | 0.310 | 0.332 | 0.321 | 36.4 | 41.4 | 77.8 |
| 6 | | 1 | 115 | 125 | 240 | 0.309 | 0.328 | 0.319 | 35.6 | 41.1 | 76.7 |
| 7 | | 2 | 101 | 77 | 178 | 0.414 | 0.482 | 0.444 | 41.7 | 37.3 | 79.0 |
| 8 | | 2 | 75 | 118 | 193 | 0.470 | 0.433 | 0.448 | 35.4 | 51.0 | 86.4 |
| 9 | | 1 | 102 | 104 | 205 | 0.317 | 0.337 | 0.327 | 32.2 | 34.9 | 67.1 |
| 10 | | 1 | 110 | 120 | 230 | 0.342 | 0.344 | 0.343 | 37.6 | 41.2 | 78.9 |
| 11 | | 2 | 127 | 119 | 246 | 0.369 | 0.424 | 0.396 | 47.1 | 50.4 | 97.5 |
| 12 | | 2 | 114 | 119 | 233 | 0.404 | 0.449 | 0.427 | 46.2 | 53.4 | 99.6 |
| Mean | | | 103 | 111 | 214 | 0.371 | 0.391 | 0.379 | 37.8 | 42.4 | 80.2 |
| S.D. | | | 15 | 18 | 26 | 0.054 | 0.073 | 0.060 | 5.3 | 6.1 | 10.2 |
| C.O.V. | | | 14% | 16% | 12% | 15% | 19% | 16% | 14% | 14% | 13% |

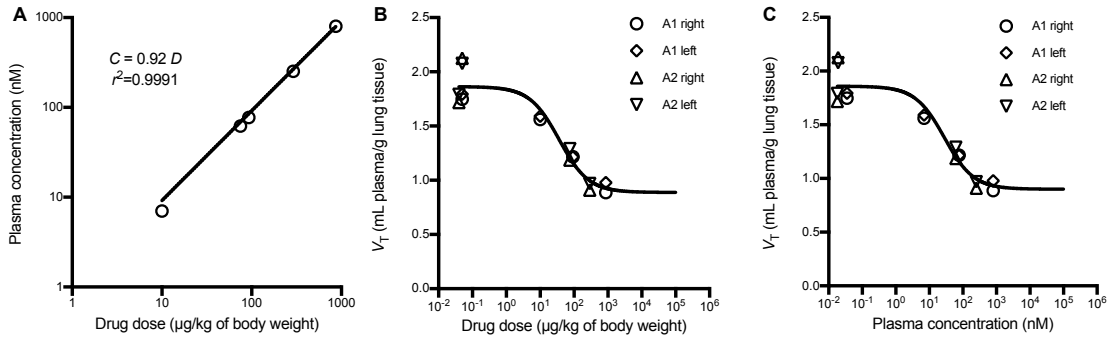


**Supplemental Figure 1**: Relationships between $^{11}$C-BMT-136088 $V_T$ value, injected mass and plasma concentration. (**A**) Relationship between $^{11}$C-BMT-136088 injected dose and plasma concentration (slope=0.92±0.01, $r^2$=0.999, $n$=5). (**B**) Relationship between $^{11}$C-BMT-136088 $V_T$ values and injected mass. (**C**) Relationship between $^{11}$C-BMT-136088 $V_T$ values and the plasma levels of BMT-136088. In **B** and **C**, the data from both animals (A1 and A2) and from both sides (right and left) of the chest could be fitted by the same curve ($F_{9,4}$=0.24, $p$=0.96 and $F_{9,4}$=0.26, $p$=0.93, respectively).

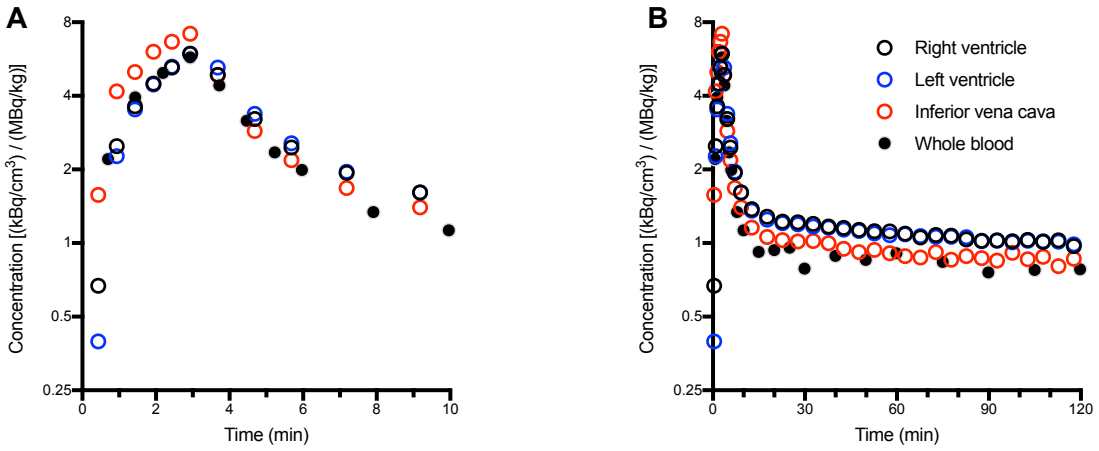


**Supplemental Figure 2**: Comparison of image derived whole blood curve with arterial data. (**A**) First 10 minutes of the curves. (**B**) Full duration of the curves. Solid symbols represent activity measured from whole blood samples. The other curves were derived from images. First pass radioactivity concentration in the vena cava is higher than other curves, likely because activity in right ventricle early samples has been diluted due to the non-radioactive blood coming from the superior vena cava. Conversely, late values in the vena cava were the closest to the arterial samples among all image-derived curves. Both ventricle curves were however higher at late times than the whole blood arterial data and the inferior vena cava curve, likely due to spill-in from the myocardium. Thus, applying partial volume correction appears necessary to use ventricle data as input for this tracer in monkeys.

**Supplemental Table 2**: Mean organ radiation dose exposure estimates from $^{11}$C-BMT-136088 in 70 kg adults male (*n*=2) and 55 kg female (*n*=2) phantoms.

| | Male | | Female | |
|---|---|---|---|---|
| **Target Organ** | **Mean** | **SD** | **Mean** | **SD** |
| Adrenals | 4.3 | 0.00 | 5.7 | 0.21 |
| Brain | 0.39 | 0.13 | 0.55 | 0.06 |
| Breasts | 1.6 | 0.14 | 1.9 | 0.18 |
| Gallbladder Wall | 9.5 | 2.4 | 13.0 | 2.7 |
| LLI Wall | 11.3 | 2.9 | 10.1 | 1.19 |
| Small Intestine | 2.4 | 0.10 | 2.7 | 0.14 |
| Stomach Wall | 2.8 | 0.35 | 3.3 | 0.21 |
| ULI Wall | 2.7 | 0.08 | 3.3 | 0.08 |
| Heart Wall | 3.9 | 0.01 | 4.8 | 0.01 |
| Kidneys | 10.8 | 3.5 | 9.1 | 0.21 |
| Liver* | 43.1 | 4.9 | 68.9 | 9.4 |
| Lungs | 6.0 | 0.50 | 5.5 | 0.04 |
| Muscle | 1.78 | 0.14 | 2.0 | 0.21 |
| Ovaries | | | 2.2 | 0.22 |
| Pancreas | 4.0 | 0.07 | 5.3 | 0.11 |
| Red Marrow | 1.8 | 0.12 | 2.0 | 0.16 |
| Osteogenic Cells | 2.1 | 0.30 | 2.5 | 0.42 |
| Skin | 1.3 | 0.16 | 1.4 | 0.21 |
| Spleen | 5.9 | 1.9 | 14.2 | 1.7 |
| Testes | 1.2 | 0.13 | | |
| Thymus | 1.7 | 0.19 | 1.9 | 0.25 |
| Thyroid | 1.3 | 0.25 | 1.2 | 0.31 |
| Urinary Bladder Wall | 7.1 | 7.4 | 5.4 | 1.4 |
| Uterus | | | 2.0 | 0.23 |
| Total Body | 2.9 | 0.02 | 3.8 | 0.02 |
| Effective Dose Equivalent | 6.9 | 0.62 | 8.7 | 0.56 |
| Effective Dose | 5.9 | 0.91 | 7.1 | 0.54 |
| Single study dose limit† (MBq) | 1160 | | 726 | |
| Effective dose equivalent for a 555 MBq injection (mSv) | 3.8 | | 4.9 | |

Values are in µSv/MBq unless specified otherwise
*Dose limiting organ
†Under CFR 361.1.1